Ocean Modelling 86 (2015) 141–152

Contents lists available at ScienceDirect

Ocean Modelling

journal homepage: www.elsevier.com/locate/ocemod

Modeling the interplay between sea ice formation and the oceanic mixed layer: Limitations of simple brine rejection parameterizations

Antoine Barthélemy [a,*], Thierry Fichefet [a], Hugues Goosse [a], Gurvan Madec [b,c]

[a] Georges Lemaître Centre for Earth and Climate Research (TECLIM), Earth and Life Institute, Université catholique de Louvain, Louvain-la-Neuve, Belgium
[b] Laboratoire d'Océanographie et du Climat: Expérimentation et Approches Numériques (LOCEAN), Paris, France
[c] National Oceanography Centre (NOC), Southampton, United Kingdom

ARTICLE INFO

Article history:
Received 8 August 2014
Received in revised form 16 November 2014
Accepted 21 December 2014
Available online 8 January 2015

Keywords:
Model
Brine rejection
Parameterization
Ocean mixed layer
Arctic
Antarctic

ABSTRACT

The subtle interplay between sea ice formation and ocean vertical mixing is hardly represented in current large-scale models designed for climate studies. Convective mixing caused by the brine release when ice forms is likely to prevail in leads and thin ice areas, while it occurs in models at the much larger horizontal grid cell scale. Subgrid-scale parameterizations have hence been developed to mimic the effects of small-scale convection using a vertical distribution of the salt rejected by sea ice within the mixed layer, instead of releasing it in the top ocean layer. Such a brine rejection parameterization is included in the global ocean–sea ice model NEMO-LIM3. Impacts on the simulated mixed layers and ocean temperature and salinity profiles, along with feedbacks on the sea ice cover, are then investigated in both hemispheres. The changes are overall relatively weak, except for mixed layer depths, which are in general excessively reduced compared to observation-based estimates. While potential model biases prevent a definitive attribution of this vertical mixing underestimation to the brine rejection parameterization, it is unlikely that the latter can be applied in all conditions. In that case, salt rejections do not play any role in mixed layer deepening, which is unrealistic. Applying the parameterization only for low ice–ocean relative velocities improves model results, but introduces additional parameters that are not well constrained by observations.

1. Introduction

Intense turbulent mixing at the surface of the ocean results in a mixed layer whose dynamics regulates the exchanges between the atmosphere and the ocean interior. In polar regions, the mixed layer development is strongly affected by the presence of sea ice. Sea ice dampens direct inputs of heat, momentum and mass from the air, while it generates buoyancy fluxes at the sea surface when it forms or melts. In turn, mixed layer characteristics impact the sea ice energy balance by modulating the oceanic heat flux at the base of the ice layer.

The large difference between seawater and sea ice salinities, the latter being much lower, implies strong brine rejections during ice formation, which may lead to destabilization and hence convective mixing of the upper portion of the water column. This subtle interplay between sea ice formation and mixing of the surface layer is currently poorly represented in large-scale ocean–sea ice models. Indeed, convection due to surface salt input occurs in models at the grid cell scale (typically from 10 to 100 km), while it is likely to prevail in the real ocean in leads and thin ice areas, at horizontal scales ranging from 100 m to a few kilometers (Duffy and Caldeira, 1997; Nguyen et al., 2009; Jin et al., 2012).

The errors caused by the misrepresentation of small-scale convection in large-scale ocean models are examined by Jin et al. (2012). In this study, a model is run on a 100 × 100 horizontal grid point domain at 1 and 30 km resolutions, and the ocean response in a 30 × 30 km box to a surface brine rejection is investigated. The box therefore consists of 30 × 30 grid points at 1 km resolution and of a single column at 30 km resolution. On the one hand, in the high resolution simulations, a localized brine rejection results in a salt plume that sinks to the bottom of the mixed layer where it spreads horizontally. The mixed layer actually shoals and the increase in salinity is greater at its base than at the surface. The same process has been observed and described in laboratory experiments and field studies (Nguyen et al., 2009, and references therein). On the other hand, in the low resolution simulations,

* Corresponding author at: Georges Lemaître Centre for Earth and Climate Research, Place Louis Pasteur 3, Box L4.03.08, 1348 Louvain-la-Neuve, Belgium. Tel.: +32 10 47 24 08.

E-mail addresses: antoine.barthelemy@uclouvain.be (A. Barthélemy), thierry.fichefet@uclouvain.be (T. Fichefet), hugues.goosse@uclouvain.be (H. Goosse), gm@locean-ipsl.upmc.fr (G. Madec).

http://dx.doi.org/10.1016/j.ocemod.2014.12.009
1463-5003/

where the salt input is by default spread out at the surface of the 30×30 km box, large-scale convection induces a deepening of the mixed layer and a vertically uniform salinity increase.

Subgrid-scale brine rejection parameterizations have been developed and included in models to address the excessive mixing issue and to mimic the effects of small-scale convection. Their basic principle is to distribute vertically the salt rejected by sea ice within or below the mixed layer, instead of releasing it in the top ocean layer. Two preliminary studies (Duffy and Caldeira, 1997; Duffy et al., 1999) distributed the salt uniformly in the upper 160 m and down to the depth where density becomes 0.4 kg/m^3 higher than at the surface. They noted improvements in the simulated intermediate and deep salinities around Antarctica, as well as in the modeled temperatures and convective activity. Subsequent implementations consisted in a power-law distribution of rejected brines within the mixed layer (Nguyen et al., 2009; Jin et al., 2012). Focusing only on the Arctic, results showed improved modeling of the Arctic cold halocline and reduction of excessive mixed layer depths. Similar ideas have also been used in the context of paleoclimate modeling. By releasing brines due to sea ice formation at the bottom of the ocean, Bouttes et al. (2010) improved the simulated carbon cycle during the last glacial maximum in an intermediate complexity climate model.

In the present study, the brine rejection parameterization scheme of Nguyen et al. (2009) is introduced into the global ocean–sea ice model NEMO-LIM3. The aim is to assess in details its effects on the mixed layer depth and properties, in both the Arctic and Antarctic, using a recently published mixed layer climatology (Schmidtko et al., 2013) and hydrographic data provided by animal-borne instruments in the Southern Ocean (Roquet et al., 2013). Because the vertical mixing scheme in NEMO is different from the one used in the above mentioned studies, this will also provide an independent confirmation or invalidation of the results previously obtained for the Arctic. Furthermore, the feedbacks triggered by the parameterization on the sea ice cover are examined.

The paper is organized as follows. The NEMO-LIM3 model, the experimental design and the brine rejection parameterization are presented in Section 2. Observational data are described in Section 3. Section 4 includes the analysis of the simulations results and a discussion of the limitations of our experiments and of the parameterization, and presents a simple method to refine the latter. A summary of our findings and concluding remarks are given in Section 5.

2. Brine rejection parameterization in the ocean–sea ice model NEMO-LIM3

2.1. Model configuration

NEMO-LIM3 is a global ocean–sea ice model routinely used in climate studies. The ocean engine of NEMO (Nucleus for European Modelling of the Ocean) is a finite-difference, hydrostatic, free-surface, primitive-equation model (Madec, 2008). It is coupled to LIM3 (Louvain-la-Neuve sea Ice Model), a dynamic-thermodynamic sea ice model with a representation of the subgrid-scale distributions of ice thickness, enthalpy and salinity (Vancoppenolle et al., 2009). The explicit inclusion of brine entrapment and drainage makes the sea ice salinity variable both in space and in time. We use version 3.5 of NEMO, with modifications to the sea ice code that include changes in the time stepping and a reformulation of ice–ocean fluxes allowing to track the different contributions to the ice mass, salt and heat balances (Rousset et al., in preparation for Geoscientific Model Development). Mesoscale eddies are parameterized following Gent and Mcwilliams (1990).

The treatment of oceanic vertical mixing is of particular interest in this study. We use the so-called TKE mixing scheme, introduced in an earlier version of the model by Blanke and Delecluse (1993) and progressively updated since then (Madec, 2008). The vertical eddy viscosity and diffusivity depend on the prognostically computed turbulent kinetic energy (TKE) and on diagnostic non-local turbulent length scales. The TKE evolves in time through production by vertical shear, destruction by stratification, vertical diffusion and dissipation. In theory, this scheme solves the issue of statically unstable density profiles in hydrostatic models because, in that case, the stratification destruction term actually becomes a source of TKE, thus yielding high mixing coefficients. An enhanced vertical diffusion scheme is however used to ensure static stability in the top ocean layers, where turbulent length scales are bounded by the distance to the surface.

Our experimental design is largely similar to the NEMO-LIM3 simulation of Massonnet et al. (2011), where additional details can be found. The model is initialized in 1948 using climatological temperature and salinity data from the World Ocean Atlas 2001 (Conkright et al., 2002), and is run until the end of 2013. The atmospheric forcing is provided by the NCEP/NCAR surface air temperature and wind reanalysis data (Kalnay et al., 1996), and by monthly climatologies for relative humidity, cloudiness, precipitation and river runoffs. Surface heat fluxes are computed following Goosse (1997), while the ice–ocean coupling is formulated as in Goosse and Fichefet (1999). Simulations are performed on the quasi-isotropic global tripolar grid ORCA1, based on the semi-analytical method of Madec and Imbard (1996), which has 1° resolution in the zonal direction. Vertical discretization is based on a partial step z-coordinate, meaning that the thickness of the bottom layer is allowed to vary to provide a better representation of the bathymetry (Adcroft et al., 1997). The thicknesses of the 46 levels otherwise range from 6 m at the surface to 20 m at 100 m depth, and reach 250 m for the bottommost layer.

Among the differences in setup compared to Massonnet et al. (2011) are the more recent model version used, tuned ice–ocean drag coefficient (from 5×10^{-3} to 3×10^{-3}) and snow thermal conductivity (from 0.31 W K^{-1} m^{-1} to 0.25 W K^{-1} m^{-1}), and a different implementation of the sea surface salinity restoring towards the PHC3 climatology (Polar Science Center Hydrographic Climatology, Steele et al., 2001). The restoring consists in a damping term in the surface freshwater budget and is necessary to avoid spurious model drift outside the polar regions. Its time scale is 310 days for a 50 m mixed layer. Here, the restoring term is multiplied by $(1 - c)$, with c the sea ice concentration. This suppresses its influence almost completely in intense ice formation areas, and ensures that the effects of the brine rejection parameterization are not altered.

2.2. Simulated sea ice in the reference experiment

Despite changes in model configuration, sea ice results remain relatively close to the ones obtained by Massonnet et al. (2011). Key figures are given in Table 1.

In the Arctic, the sea ice extent mean seasonal cycle is well reproduced compared to observations (Comiso, 2000), showing only a positive bias around 1×10^6 km^2 throughout the year. The ice volume appears significantly overestimated with respect to the PIOMAS reanalysis using data assimilation (Pan-Arctic Ice Ocean Modeling and Assimilation System, Schweiger et al., 2011), but the offset is essentially caused by spurious ice accumulations in narrow straits in the Canadian Arctic Archipelago, not accurately represented in the model at 1° resolution. The phase and amplitude of the ice volume seasonal cycle actually closely match the PIOMAS data. Finally, both ice extent and volume trends are in very good agreement with observations and reanalysis estimates.

In the Southern Hemisphere, the main discrepancy with available observations is an underestimation of the amplitude of the

Table 1
Sea ice metrics in observations or reanalyses, and in the reference (REF) and BRP experiments (see Table 2 for details). Sea ice extent is compared between 1983 and 2012 with passive microwave products generated with the Bootstrap algorithm (Comiso, 2000). Arctic sea ice volume estimates are from the PIOMAS reanalysis (Schweiger et al., 2011) over the 1983–2013 period. The Antarctic sea ice volume trend is from the model reconstruction by Massonnet et al. (2013) between 1980 and 2008.

	Arctic			Antarctic		
	Obs./reanalysis	REF	BRP	Obs./reanalysis	REF	BRP
Max. monthly extent (10^6 km^2)	15.5	16.5	16.5	19.2	18.4	18.6
Min. monthly extent (10^6 km^2)	6.7	7.7	7.7	3.2	6.2	5.8
Trend extent (10^3 km^2 year^{-1})	−53	−58	−57	+21	+37	+36
Max. monthly volume (10^3 km^3)	27.8	33.3	33.2	n/a	14.4	14.1
Min. monthly volume (10^3 km^3)	11.2	17.3	17.2	n/a	3.7	3.3
Trend volume (km^3 year^{-1})	−346	−374	−377	+36 ± 34	+83	+66

ice extent seasonal cycle, especially at the summer minimum. The simulated upward trend in sea ice extent is also too large, as is the trend in ice volume against the model reconstruction with data assimilation by Massonnet et al. (2013). Compared to the ASPeCt dataset based on shipboard observations (Antarctic Sea ice Processes and Climate, Worby et al., 2008), the model tends to overestimate the sea ice thickness, except northeast of the Antarctic Peninsula and along the coasts of East Antarctica and eastern Ross Sea, where the opposite occurs. The mean absolute error in ice thickness is 43 cm.

This brief evaluation of the sea ice results in the reference experiment shows that NEMO-LIM3 is clearly appropriate to study the impacts of a brine rejection parameterization on the oceanic component of the system. The model skill in the representation of this latter component is discussed in Section 4 together with the changes induced by the parameterization. Nevertheless, we note that Antarctic sea ice does not melt enough in summer in the model, which could lead us to underestimate the parameterization effect in the Southern Ocean when ice freezes up again in autumn.

2.3. Brine rejection parameterization

In the standard model configuration, all surface fluxes linked to the presence of sea ice are applied in the first ocean layer. In order to mimic small-scale convection associated with sea ice formation, brine rejection parameterizations (BRP) distribute the rejected salt directly within the mixed layer. Owing to its positive buoyancy, low salinity water resulting from sea ice melt is always placed in the uppermost layer.

Based on salt plume physics, laboratory and numerical experiments, Nguyen et al. (2009) found the optimal brine vertical distribution $s(z)$ to be a power law:

$$s(z) = \begin{cases} Az^n & \text{if} \quad z \leqslant D \\ 0 & \text{if} \quad z > D \end{cases}$$

where z is depth, A a normalizing factor equal to $\frac{n+1}{D^{n+1}}$, D a measure of the mixed layer depth (MLD) and $n = 5$. The large n implies that most of the salt is rejected at the bottom of the mixed layer. The same value was found independently by Jin et al. (2012) for small leads using their high resolution model. Since the shape of the distribution seems well constrained, we only test here the sensitivity of the BRP to the distribution maximum depth.

Nguyen et al. (2009) took D as the depth corresponding to a density gradient of 0.02 kg m^{-4}. Jin et al. (2012) rather used the MLD provided in their model by the turbulence k-profile parameterization. In NEMO, the mixed layer base is determined by default by a density difference of 0.01 kg m^{-3} compared to the value at 10 m depth, which is the second oceanic level in our vertical discretization. This low density threshold is found to be appropriate to identify the almost perfectly homogeneous simulated mixed layers. An additional diagnostic, based on the 0.03 kg m^{-3} threshold recommended by de Boyer Montégut et al. (2004) for observed density profiles, is also implemented. These mixed layers depths are denoted MLD.01 and MLD.03, respectively. Besides the reference simulation where the BRP is disabled, four sensitivity experiments are performed, in which the BRP is turned on and D is set to one level above MLD.01, MLD.01, one level below MLD.01 and MLD.03. The latter corresponds almost everywhere to the deepest distribution. A sixth experiment, in which the BRP is only activated for low ice–ocean relative velocities, is mentioned here for completeness and is further discussed in Section 4.3. The experiments are summarized in Table 2.

An important hypothesis, made here as well as in all previous studies, is that all the salt is rejected by sea ice in a localized manner (for instance in leads). This amounts to saying that all the salt originating from sea ice has to be handled with the parameterization, thus distributed vertically.

3. Observational data

Observational data used to validate the ocean model results come from two sources: the MIMOC climatology (Monthly Isopycnal and Mixed layer Ocean Climatology) and the MEOP-CTD hydrographic dataset (Marine Mammals Exploring the Oceans Pole to Pole).

The MIMOC global upper-ocean climatology (Schmidtko et al., 2013) is based on conductivity–temperature–depth (CTD) profiles from the World Ocean Database (i.e., shipboard data), Argo floats and automated Ice-Tethered Profilers (ITP). The inclusion of the latter increases dramatically the number of upper-ocean observations in the Arctic Ocean, in all seasons, since 2004 (Krishfield et al., 2008). The MIMOC product includes MLDs computed from individual profiles with the Holte and Talley (2009) algorithm. We use the weighted mean monthly fields.

In the Southern Ocean, most of the observations used to construct the MIMOC climatology come from summertime cruises, because Argo floats can hardly sample the ocean beneath sea ice and because there is no equivalent to the ITP project in the Antarctic. Therefore, we also compare our results with the MEOP-CTD dataset (Roquet et al., 2011, 2013), a calibrated compilation of temperature and salinity (T/S) profiles collected by hundreds of seals

Table 2
List of sensitivity experiments.

Experiment	Parameterization	Maximum depth D
REF	No	–
BRP-1	Yes	1 Level above MLD.01
BRP	Yes	MLD.01
BRP + 1	Yes	1 Level below MLD.01
BRP_3	Yes	MLD.03
BRPv	For low ice–ocean relative velocities	MLD.01

equipped with CTD sensors between 2004 and 2011. These seal-derived data are nowadays the largest source of hydrographic information south of the Antarctic Circumpolar Current (ACC). A MLD climatology is built from the dataset in the following way.

For each profile, the MLD.01 and MLD.03 are computed as in the model, except that the reference density value is taken at 15 m depth. This is very often the first available T/S value in the profile. Profiles without data at this depth are rejected. In some cases, the required density difference is not reached until the deepest T/S measurement, because the seal did not reach the mixed layer base or because the mixed layer extended down to the seafloor. Including such profiles barely changes the resulting climatology, hence we keep the maximum depth with data as a lower limit for the MLD. Finally, for each ORCA1 grid cell and each month, the available MLD values are averaged to obtain the climatology. In the following figures, all grid points with data are plotted on maps, while only those with at least 5 MLD values are shown on scatter plots, in order to reduce the uncertainty associated with poorly sampled regions in the seal-derived data.

A comparison between MIMOC and MEOP-CTD MLDs in the Southern Ocean is shown in Fig. 1. As a reminder, MIMOC MLDs are computed thanks to the Holte and Talley (2009) algorithm. When comparing their algorithm outputs with the 0.03 kg m^{-3} density threshold method for Argo profiles (i.e., not under sea ice), they show that the latter slightly overestimates MLDs. We choose to compare the MIMOC climatology with MLD.01 from the MEOP-CTD data, since this stricter criterion appears better suited for the weakly stratified under-ice ocean in the Southern Hemisphere.

In Fig. 1a, a reasonable agreement between MIMOC and MEOP-CTD is obtained in the open ocean, while the MLDs are severely underestimated by MIMOC over continental shelves (how we define exactly these regions is explained in the next section). The slopes of the least squares linear fits shown in the figure and the correlation coefficients are, respectively, 0.93 and 0.62 in the open ocean, and 0.33 and 0.49 on the shelves. Maps are shown for May (Fig. 1b–d), as a compromise between deepening mixed layers and decreasing seal data coverage towards winter. They confirm that the errors between the two climatologies are generally smaller than 30 m away from the continent, but that MIMOC misses the deep MLDs along the coast of East Antarctica, by more than 150 m in several places. Note that this underestimation would have been even larger if we had used the MLD.03 criterion for MEOP-CTD, which would have yielded deeper mixed layers for this dataset.

4. Results and discussion

The NEMO-LIM3 response to the introduction of a brine rejection parameterization is now explored in both polar regions, as well as the model sensitivity to the choice of the vertical distribution depth. We examine model outputs averaged over the 1983–2013 period, except for the evaluation against the MEOP-CTD dataset, for which the 2004–2011 period is considered.

In what follows, some diagnostics are performed over three selected areas (Fig. 2). Large changes occur in the central part of the Arctic Ocean, hence we identify the "Arctic Basin" (AB) as the region enclosed by the 500 m isobath and the 80°N parallel in Fram Strait (with a limited number of adjustments to avoid isolated grid cells). In the Antarctic, we distinguish between the "Antarctic open ocean" (AOO) and the "Antarctic shelves" (AS), based on the large differences in sea ice production rates and associated mixed layer regimes. The limit between both areas is normally the 1000 m isobath. However, the net ice growth over the Amundsen and Bellingshausen Seas shelves is much lower than in the Ross Sea

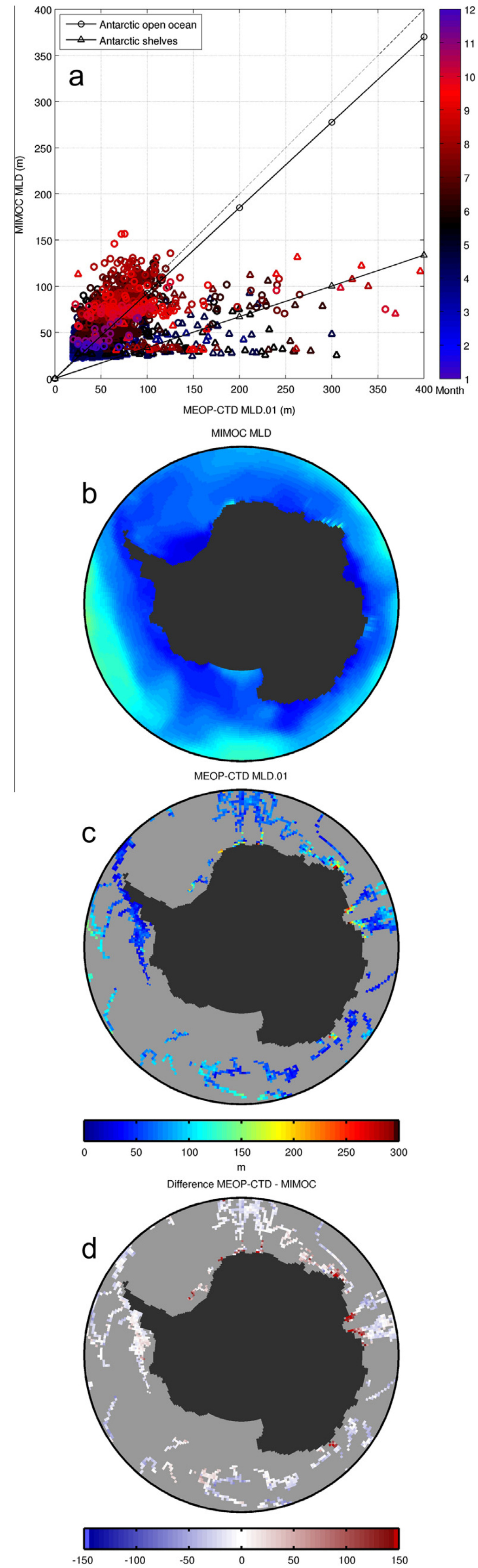

Fig. 1. Comparison of MIMOC and MEOP-CTD MLDs. Scatter plot of MIMOC MLD versus MEOP-CTD MLD.01 (a), and maps of MIMOC MLD (b), MEOP-CTD MLD.01 (c) and their difference (MEOP-CTD – MIMOC, d) in May. In the scatter plot, a distinction is made between the points in the Antarctic open ocean and over the Antarctic shelves, solid lines are least squares linear fits and the dashed line is the diagonal.

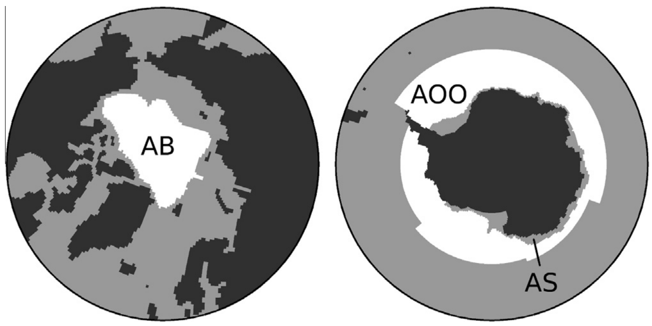

Fig. 2. Selected areas for the results analysis: Arctic basin (AB), Antarctic open ocean (AOO) and Antarctic shelves (AS).

for instance, implying shallower MLDs (Petty et al., 2014). These shelf regions, along with the northern part of the Antarctic Peninsula, are excluded from AS. The northern limit of AOO is chosen as to ensure that the largest fraction of the area is covered with sea ice in winter.

In addition to the MLD.01 and MLD.03, the model also provides the turbocline depth (TCD). It is defined as the depth at which the vertical eddy diffusivity given by the TKE scheme falls below a given value, namely 5 cm/s^2. As a consequence, the turbocline is the actively mixing layer at the surface of the ocean, while MLD.01 and MLD.03 are only weakly stratified layers, i.e. mixed layers.

4.1. Arctic Ocean

The main impact of the BRP inclusion in the model is a dramatic reduction in mixed layer depths (except in late summer), clearly seen from their spatially-averaged seasonal cycles shown in Fig. 3a and b. The deeper the vertical salt distribution, the larger the effect. This result is not surprising and is in line with previous studies (Nguyen et al., 2009; Jin et al., 2012). In the absence of sea ice, upper-ocean mixing is caused by wind stirring and/or by surface heat losses. The presence of sea ice lessens the role of these processes, leaving negative buoyancy fluxes linked to brine rejection as the main reason for mixed layer deepening. This has been shown explicitly by Petty et al. (2014) for Antarctic continental shelves. The BRP not only suppresses this deepening mechanism, but also restratifies the mixed layer, since salt is distributed according to an increasing function of depth.

The comparison between the model results and the MIMOC climatology is not direct because of the various MLD definitions used. Without BRP, the different criteria in the model agree within 10 m at the winter maximum, and overestimate the MIMOC value by 10 to 25 m. Summer minima, on the other hand, are constantly underestimated. This latter bias, common in current climate models and possibly caused by a poor or missing representation of mixing processes like surface waves and Langmuir circulations (Huang et al., 2014), is beyond the scope of the present paper. When the BRP is introduced, the gap widens between the MLDs obtained from the three criteria in the model. The TCD undergoes the largest decrease and becomes in all cases close to the minimum allowed model value (12 m). The MLD.03 is significantly affected only when the brine distribution depth is the MLD.03 itself. The MLD.01, which we consider the best characterization of the almost perfectly homogeneous modeled mixed layers, is excessively reduced compared to MIMOC, although the amplitude of the seasonal cycle fits the climatology better, in particular for experiment BRP.

Maps of MLDs in March are shown in Fig. 4 for MIMOC and for MLD.01 in experiments REF and BRP. Mixed layers exceeding 100 m occur in REF around Greenland and in the east part of the Canadian Arctic Archipelago, as well as in the western Labrador Sea and the Hudson Bay, in stark contrast to observations. These biases compared to MIMOC are effectively reduced in BRP. Besides, the maps confirm the excessive MLD decrease in the Arctic basin shown in Fig. 3. On average, there is a switch from an overestimation of the order of 15 m in REF to an underestimation of around 10 m in BRP with respect to MIMOC.

The mean upper-ocean vertical temperature and salinity profiles in March are plotted for all experiments in Fig. 5a and d. As for MLDs, the BRP effect is larger when the maximum distribution depth is greater, but their overall shape remains largely unchanged, as would be a comparison with observed data. The sea surface salinity (SSS) decreases by less than 0.05 psu on average in the AB area in experiment BRP compared to REF. Salinity below 20 m tends to marginally increase when the BRP is activated, as expected from the design of the parameterization.

Sea surface temperature (SST) is forced to remain close to the freezing point due to the presence of sea ice, itself strongly constrained by the atmospheric forcing. In the subsurface, a warming of the water column is noted when the BRP is activated. This is explained by the weaker vertical mixing, which reduces the upward heat transfer in the ocean and therefore lowers the heat losses to the atmosphere active in autumn and winter. The warming is maximum between 15 and 30 m and vanishes below 100 m. On average in the upper 100 m, the temperature is 0.02 °C higher in BRP than in REF from autumn to spring. To a large extent, the difference persists in summer. The reason why changes remain limited is the near freezing temperatures characterizing the cold halocline in the Arctic Ocean, well visible in the upper 40 m of the mean profile in Fig. 5a but extending deeper in certain areas. Such a subsurface warming is also noticeable in the results of Nguyen et al. (2009).

As mentioned by Jin et al. (2012), the effects of the BRP on Arctic sea ice are weak. The parameterization slightly enhances the oceanic heat flux at the ice base, through a mechanism that will be described in more details for the Southern Ocean, where the signal is stronger. In the Arctic, given the prescribed atmospheric forcing used by the model, the change is too small to influence markedly the sea ice cover. The latter is indeed nearly identical in all experiments. Figures are shown for REF and BRP in Table 1.

Besides some similarities between our results and those of Nguyen et al. (2009) and Jin et al. (2012), two important differences are also noted. First, while the reductions in mixed layer thickness following the introduction of the BRP are of the same order of magnitude, neither of those studies concludes to an excessive MLD decrease. This is essentially due to their reference experiment having positive biases in MLD compared to observations that are clearly larger than ours. Second, the changes in vertical T/S profiles appear much smaller in our results. This difference in ocean response is at least partly explained by the higher background vertical diffusivity used in our model setup (1.2×10^{-5} m/s^2 against 1×10^{-6} m/s^2, see also Section 4.3).

4.2. Southern Ocean

In the REF experiment, one prominent feature of the under-ice winter mixed layer is the deep MLDs simulated in the Ross and Weddell Seas (Fig. 4f). These reach 500 m along the ice shelves, which implies the destratification of a significant fraction of the water column and the production of dense cold and saline waters over the continental shelves. MLDs close to and locally exceeding 200 m also occur along the coast of East Antarctica. Lower sea ice formation rates imply lower MLDs in the Amundsen and Bellingshausen Seas and around the northern tip of the Antarctic Peninsula. This MLD pattern is most similar with other recent modeling studies (Petty et al., 2014; Holland et al., 2014).

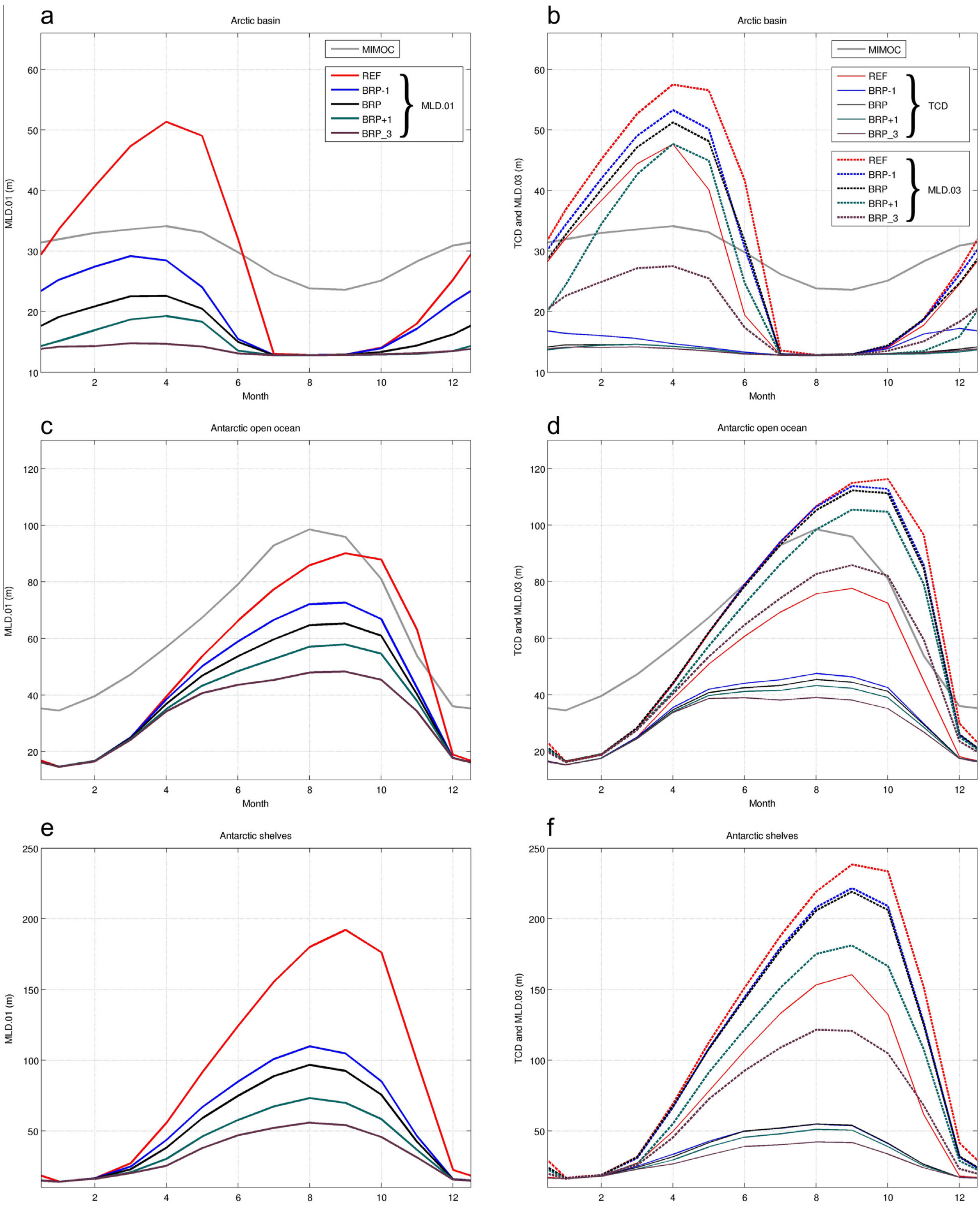

Fig. 3. Seasonal cycles of mixed layer and turbocline depths, for the MIMOC climatology and model experiments, in the Arctic basin (a, b), Antarctic open ocean (c, d) and Antarctic shelves (e, f) areas. MLD.01s are shown as thick solid lines (left), and TCDs and MLD.03s as thin solid lines and as dashed lines, respectively (right). Following the discussion in Section 3, the MIMOC climatology is not plotted for the Antarctic shelves area.

The agreement between model mixed layers and observations is relatively good in the Antarctic open ocean area. The spatially-averaged model MLD.01 winter maximum is less than 10 m smaller than the MIMOC value of 100 m, and it occurs one month later (Fig. 3c). This slight underestimation is confirmed by a comparison with the MEOP-CTD data (Fig. 6a and c). Over the Antarctic continental shelves, where we have shown that the MIMOC MLDs are unrealistic (Section 3), we consider only the seal-derived data. In this area, the mean model MLD.01 reaches as much as 190 m in September (Fig. 3e). Fig. 6a shows that it might still be underesti-

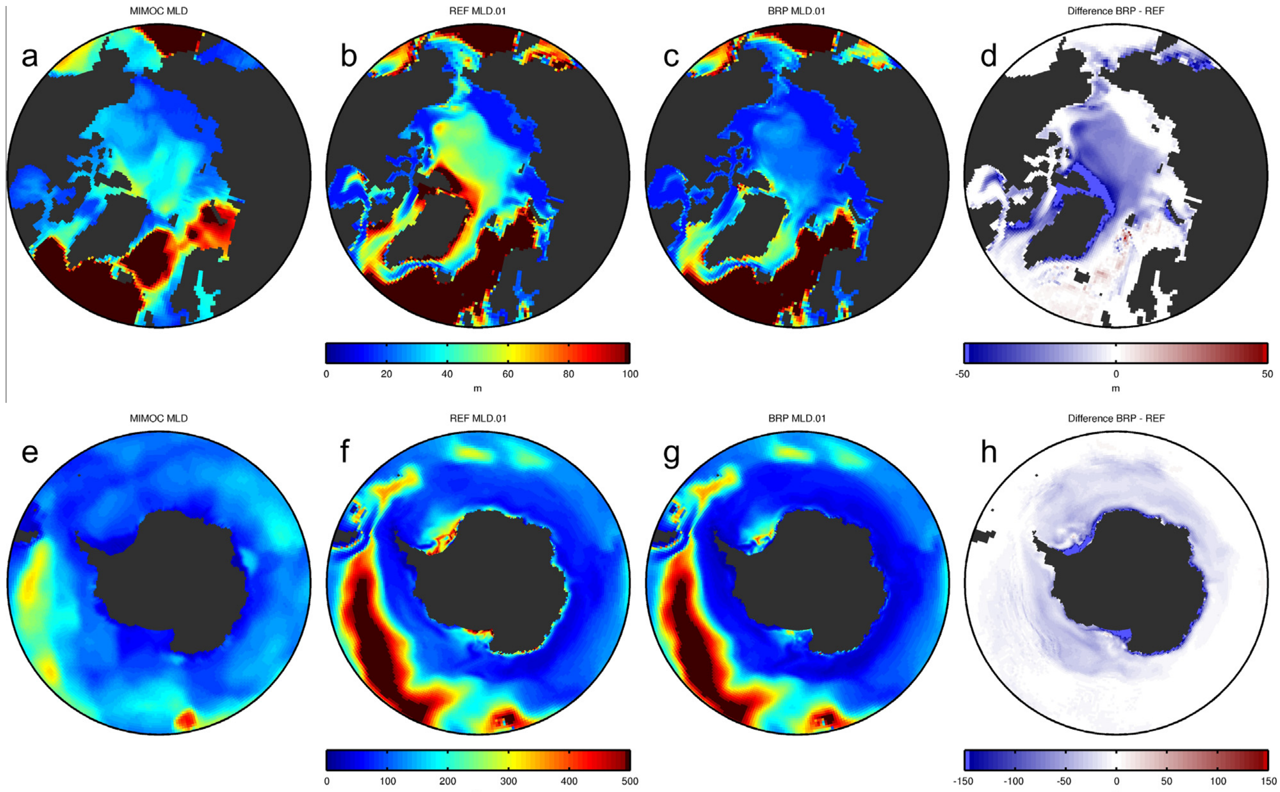

Fig. 4. MIMOC MLDs (a, e) and model MLD.01s for experiments REF (b, f), BRP (c, g) and their difference (BRP – REF; d, h). Blue (red) areas in panels (d) and (h) correspond to shallower (deeper) mixed layers in BRP compared to REF. Maps are shown for March in the Northern Hemisphere and for September in the Southern Hemisphere. (For interpretation of the references to color in this figure legend, the reader is referred to the web version of this article.)

mated on average compared to reality. The map for May in Fig. 6c indicates that too shallow MLDs occur along the coast of East Antarctica, but that the model mixed layer is too deep in the Weddell Sea. No data is available in the Ross Sea. Finally, the summer MLD problem is also present in the Southern Ocean, as well as a strong positive bias in MLDs in the ACC in the Pacific and Atlantic Oceans (Fig. 4e and f).

As in the Northern Hemisphere, including the BRP results in a significant mixed layer shallowing in ice-covered areas. Again, the effects are more pronounced for deeper brine distributions and for the turbocline depth (Fig. 3c–f). The maximum value of the average TCD is indeed less than 50 m in all experiments with the BRP, while it is not too different from MLD.01 in the reference experiment. In the Antarctic, MLD reductions are stronger in regions where much sea ice forms, reaching there often more than 150 m for MLD.01 (Fig. 4f–h).

Given the relatively good mixed layer representation in the ice-covered areas of the Southern Ocean in the REF experiment, the BRP inclusion degrades the model performance by yielding too shallow MLDs. The issue is especially clear over the continental shelves. The spatially-averaged MLD.01 in the AS region decreases by almost 100 m in September for experiment BRP (Fig. 3e). The reductions mostly occur in areas where the MLD was already underestimated in REF, whereas the simulation is only partly improved in the Weddell Sea (Fig. 6b and d). In AOO, for the same experiments, the MLD.01 diminishes by more than 20 m on average in September, leading to an underestimation of the seasonal cycle maximum by more than 30 m with respect to MIMOC. (Fig. 3c).

Consistently with the MLD changes, the BRP impacts on the mean vertical salinity and temperature profiles in September are larger in the AS area than in AOO (Fig. 5). The decrease in SSS is less than 0.01 psu in experiment BRP compared to REF in AOO, while it is 0.03 psu in AS. The increase in salinity in the subsurface between these two experiments reaches 0.01 psu at 60 m depth in AOO and the same value at 300 m in AS. The difference becomes much smaller in AOO below 200 m. The analysis of the mean response below 400 m depth in AS becomes gradually less significant due to the diminishing number of grid points participating in the average.

As in the Arctic, reduced vertical mixing in autumn and winter in simulations with the BRP induces a warming of the water column, except at the surface which remains at the freezing point. Changes are however larger due to the presence of warmer water below the surface layer in the Southern Ocean. The temperature is up to 0.1 °C higher in experiment BRP compared to REF at 60 m depth in AOO, while the difference is fairly constant at almost 0.15 °C in the upper 400 m in AS. These changes, originating in MLD differences in the winter season, are partly maintained in summer.

The link between sea ice-related surface processes and bottom ocean properties in the Antarctic has long been recognized (e.g., Goosse and Fichefet, 1999). Given the previous results, the inclusion of the BRP is expected to have an influence on the cold and saline waters present on the continental shelves around Antarctica. The bottom temperature indeed increases by more than 0.2 °C in the Weddell and Ross Seas and along the coast of East Antarctica, and the bottom salinity by up to 0.03 psu in the Ross Sea (not shown). These changes do not help reducing the model biases of deep ocean properties. The Antarctic Bottom Water body also becomes warmer and saltier in experiment BRP, but the length of our simulations does not allow us to be conclusive on this matter.

The ocean changes caused by the introduction of the BRP are sufficient to affect sea ice, through modifications of the oceanic heat flux at its base, in spite of the prescribed atmospheric forcing.

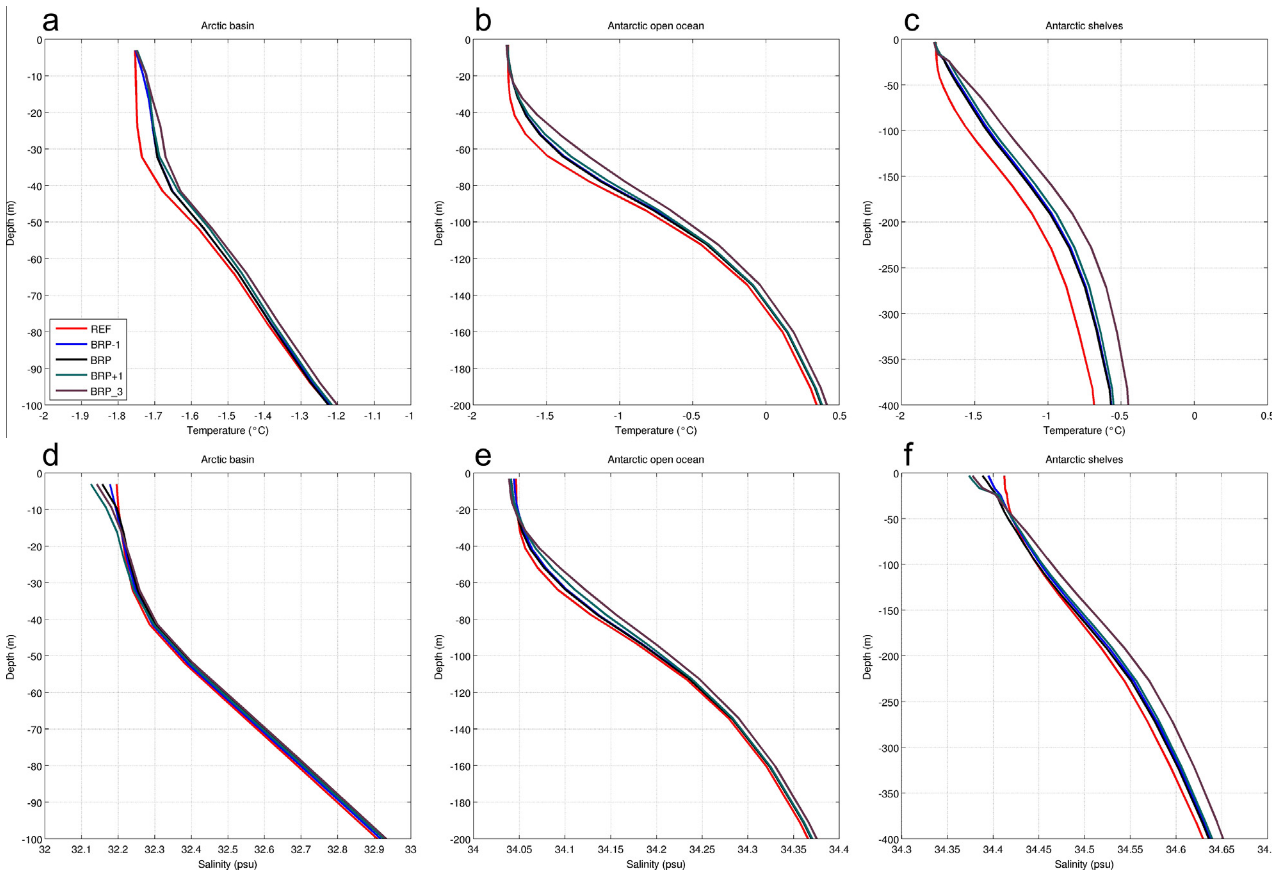

Fig. 5. Mean model temperature and salinity profiles in the Arctic basin (a, d), Antarctic open ocean (b, e) and Antarctic shelves (c, f) areas, for March in the Northern Hemisphere and for September in the Southern Hemisphere.

Reducing the vertical mixing has two competing effects on this flux. On the one hand, less mixing tends to lower the upward heat transfer from the ocean subsurface to the ice, thus reducing the heat flux. On the other hand, smaller heat losses to the atmosphere in autumn and winter have been shown to increase the upper-ocean temperature. Yet, during winter, vertical mixing events, such as those induced by storms, are able to transfer heat from this layer to the sea ice base (Jackson et al., 2012; Zhang et al., 2013). This process is associated with a larger heat flux when the subsurface is warmer, as in BRP.

Looking at the heat flux maps in September for experiment BRP and at differences with REF (Fig. 7c and d), we note that the first effect dominates in coastal areas undergoing intense heat flux in the reference experiment. Elsewhere, the second effect prevails, resulting in a higher heat flux when the BRP is included. The combined influence of these changes and of ice advection patterns explains the differences in sea ice thickness between experiments BRP and REF (Fig. 7a and b). For instance, the smaller heat fluxes encountered in the eastern Weddell Sea generate positive ice thickness anomalies that are transported along the Filchner-Ronne Ice Shelf and the Antarctic Peninsula by the cyclonic gyre existing in this region. Overall, sea ice is generally thicker along the coast, by up to 0.2 m, while it is thinner in the open ocean, mainly in the Pacific and Atlantic sectors, where the decrease reaches 0.2 m. Because thinner ice retreats further south in summer, and because the shallower mixed layer has a smaller inertia in winter, the seasonal cycle of ice extent is slightly stronger in experiment BRP, by 0.6×10^6 m^2 (Table 1). Nonetheless, for both the thickness and the extent, the changes are insufficient to correct the model errors compared to observations.

4.3. Limitations of the approach and simple refinement of the parameterization

Field and numerical studies have shown that the salt rejected during intense sea ice formation at the surface of a slowly moving lead mainly settles at the base of the mixed layer, instead of being incorporated uniformly within it (Smith and Morison, 1998; Morison and McPhee, 1998; Matsumura and Hasumi, 2008; Jin et al., 2012). As a consequence, the mixed layer is made shallower and more stratified. This provides a sound physical basis for the brine rejection parameterization proposed by Nguyen et al. (2009).

It may therefore appear surprising that the introduction of the BRP does not systematically provide a closer match between our model results and observations. In the Arctic, mixed layer depths are better simulated with a BRP only around Greenland and in the east part of the Canadian Arctic Archipelago, the western Labrador Sea and Hudson Bay. Anywhere else, namely inside the Arctic Ocean and in the Antarctic, MLDs are excessively reduced in simulations with a BRP compared to climatologies and hydrographic products. This is particularly obvious over the continental shelves around Antarctica.

Another feature of interest in the model results is the enhanced gap that appears when the BRP is activated between the MLDs computed from density threshold methods and the TCD. Under growing sea ice, vertical mixing in the upper ocean is mainly due to convection caused by negative buoyancy fluxes linked to brine rejection. The BRP suppresses this effect, resulting in a very low vertical mixing. This is immediately reflected in the depth of the turbocline, the latter being by definition the layer of active mixing. By contrast, as defined in this study, the MLD decreases only if

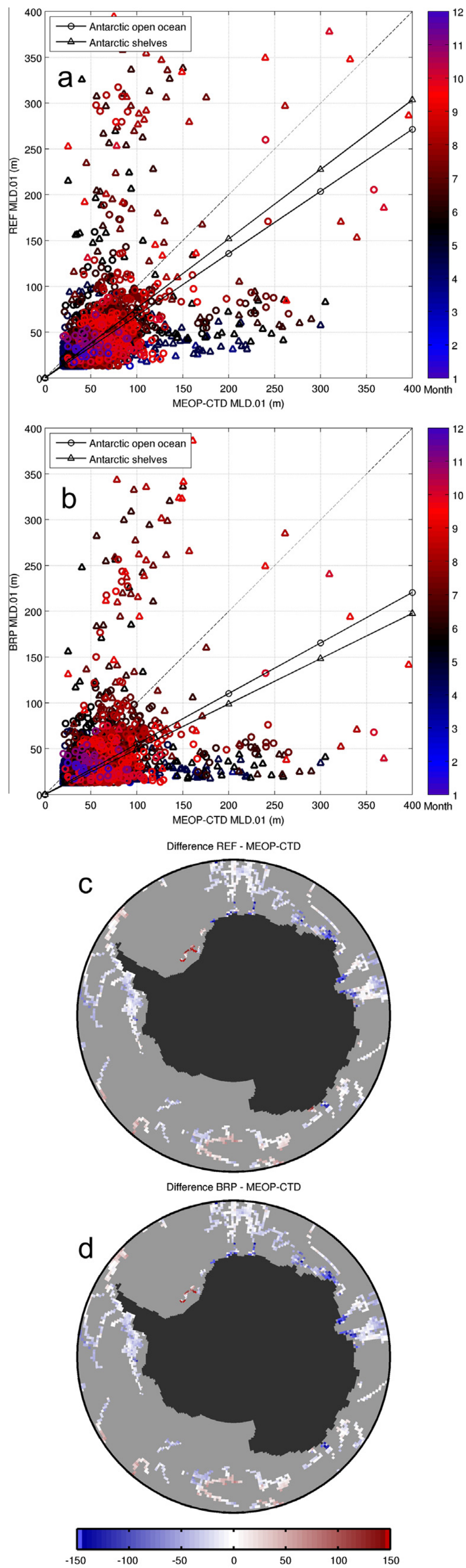

Fig. 6. Comparison of MEOP-CTD and model MLDs. The MLD.01 is shown in all cases. Scatter plots of MEOP-CTD versus REF (a) and BRP (b) experiments, and maps of differences REF – MEOP-CTD (c) and BRP – MEOP-CTD (d) in May. In the scatter plots, a distinction is made between the points in the Antarctic open ocean and over the Antarctic shelves, solid lines are least squares linear fits and the dashed line is the diagonal.

restratification takes place. The stratification visible close to the surface in vertical profiles in ice-covered regions (Fig. 5) is a sign of an extremely shallow mixing layer, but is too weak to diminish the MLDs as much as the TCD (Fig. 3). In a broader perspective, the lack of vertical mixing would be problematic if NEMO was coupled to a biogeochemical model. This would indeed impede vertical replenishment of nutrients and strongly alter surface biogeochemical cycles (e.g., Vancoppenolle et al., 2013; Smith et al., 2014).

Since the BRP can only reduce MLDs, whether the parameterization improves the comparison with observations actually depends on the model mean state. Consequently, an evaluation of the parameterization is inevitably linked to the biases present in the standard version of the model. We have already mentioned in Section 4.1 that poorly-represented or missing processes, among which surface waves and Langmuir circulations, could explain shortfalls in simulated vertical mixing during summer (Huang et al., 2014). The biases that we have pointed out in winter in simulations with a BRP could hence also originate in the absence or misrepresentation of such mixing sources. In particular, the NEMO TKE scheme includes parameterizations of near-inertial wave breaking and Langmuir turbulence, but they require further testing and development (Calvert and Siddorn, 2013; Rodgers et al., 2014), and potentially some adaptations in ice-covered oceans. Moreover, no submesoscale eddy parameterization is activated in our model configuration, although the primary impact would anyway be a shoaling of the mixed layer, especially in polar winter regions (Fox-Kemper et al., 2011).

The background vertical diffusivity is one key model parameter that could as well influence our conclusions. This diffusivity is used to account for unresolved and otherwise unparameterized mixing processes. Lowering its value has been shown to improve Arctic Ocean simulations, in models using both the turbulence k-profile parameterization (Zhang and Steele, 2007; Nguyen et al., 2009) or TKE mixing schemes (Komuro, 2014). As a test, the experiments REF and BRP have been repeated with a tenfold reduction of the background vertical diffusivity poleward of 60° N and of 60° S. The reference value (1.2×10^{-5} m/s^2) was maintained between 50° N and 50° S, with linear transitions between the different sectors. While results are barely affected in the Antarctic, the model mean state in the Arctic is indeed significantly impacted. Under-ice mixed layers shoal rather uniformly. As a result, the regions where the BRP improves the agreement with observations are more limited, and the MLDs underestimation in other regions is more pronounced. The behavior of the parameterization itself is nonetheless unchanged.

In spite of the reservations expressed above about the attribution of biases to the BRP, it is doubtful that the parameterization can be applied in all conditions to all the salt rejected by sea ice. This simplification, also used in previous studies, totally suppresses the potential of brine rejections to deepen the mixed layer. With the BRP turned on, their effect becomes on the contrary to weakly restratify the mixed layer, which is unrealistic.

Firstly, although in the wintertime open waters undergo the highest heat losses to the atmosphere and hence the highest freezing rates (Maykut, 1978), only a fraction of the ice volume is formed in leads. The remaining fraction is produced at much larger horizontal scales, in particular by bottom accretion below the existing ice cover. As noted by Jin et al. (2012), the BRP becomes unnecessary for such widespread salt input at the ocean surface, for which the model vertical mixing scheme is likely to work properly. Identifying the part of the brine that is rejected in a localized manner and has to be handled with the BRP is, however, not easy. Using the BRP only for the salt rejected in the open-water fraction of the grid cell barely changes the model results compared to the reference experiment (not shown). This is because openings within

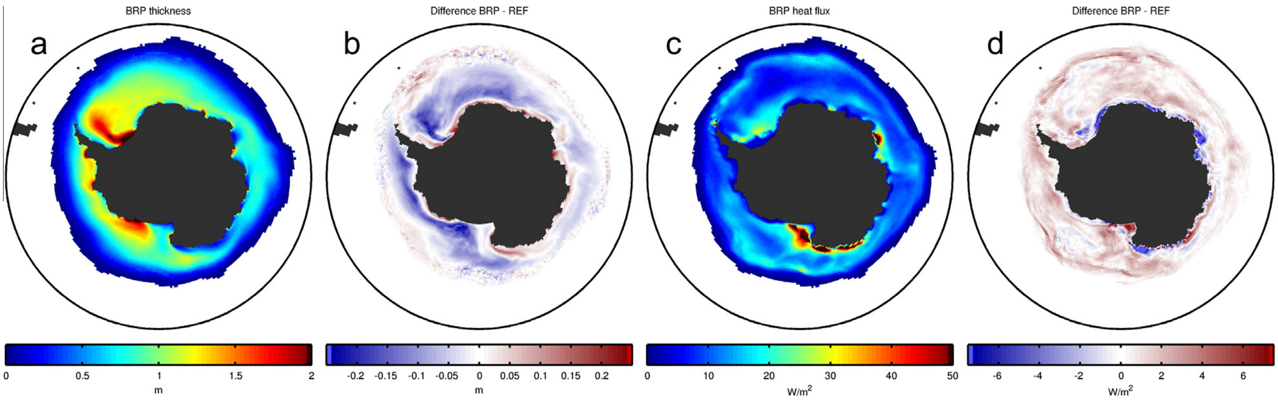

Fig. 7. September sea ice thicknesses (a) and oceanic heat fluxes (c) in experiment BRP, and differences with experiment REF (BRP – REF; b, d). Red (blue) areas in panels (b) and (d) correspond to thicker (thinner) ice or higher (lower) heat flux in BRP. (For interpretation of the references to color in this figure legend, the reader is referred to the web version of this article.)

the sea ice cover refreeze quickly, making the open-water fraction and the associated sea ice production very low.

Secondly, studies based on field observations and on model results have shown that ice–water relative velocities higher than 5 cm s^{-1} prevent the formation of salt plumes (Morison et al., 1992; Smith and Morison, 1993; Muench et al., 1995; Kantha, 1995; Skyllingstad and Denbo, 2001). In that case, mixing generated by shear turbulence dominates convective mixing, the salt rejected at the surface simply mixes into the mixed layer and the application of a BRP is not appropriate. This might explain why results are not as problematic in the Arctic as below the faster-moving Antarctic sea ice.

Finally, it is not clear whether the BRP is valid for the very deep MLDs encountered over the Southern Ocean continental shelves. Although these parameterizations were at first developed for the Antarctic (Duffy and Caldeira, 1997; Duffy et al., 1999), it would be surprising that salt plumes generated by narrow leads reach the mixed layer base situated several hundred meters below the surface. Other types of convection schemes have been proposed to address specifically the problem of deep convection (Kim and Stössel, 2001). Applying such methods might yield better results than the BRP tested here in deep mixed layer areas.

Among the three issues raised above, testing a parameterization including a dependency on the ice–ocean relative velocity appears to be the most straightforward and instructive. Accordingly, an additional experiment called BRPv is performed, corresponding to the simulation BRP with the parameterization only active for low velocities. In practice, the instantaneous ice–ocean relative velocity is used to compute the fraction of the rejected salt that is handled with the BRP. This fraction is 1 below 2.5 cm/s and 0 above 7.5 cm/s, and increases linearly between these two values. The remaining salt fraction is rejected in the top ocean layer. Results are shown in Fig. 8.

In the Arctic, the parameterization is applied in the same way as in the BRP experiment in and north of the Canadian Arctic Archipelago, in Baffin Bay and in sparse coastal sectors. Besides, between 50% and 100% of the rejected salt is distributed vertically in most of the Arctic Ocean, where it allows to recover MLDs that are closer to the MIMOC climatology. On average in the AB area, the winter maximum of MLD.01 is still underestimated by 5 m in BRPv with respect to MIMOC (not shown). The BRP finally does not apply east of Greenland and in the Labrador Sea, where the model biases present in the reference simulation therefore reappear. In the Antarctic, the BRP is only applied in very limited coastal areas, and to less than 50% of the rejected salt in parts of the Weddell and Ross Seas. As a consequence, MLDs are much less reduced in BRPv than in BRP, the best match with observations being nevertheless still provided by REF.

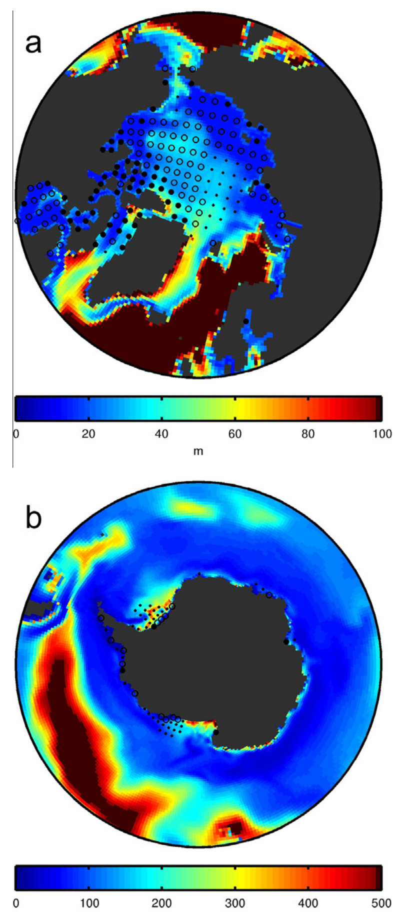

Fig. 8. MLD.01s in model experiment BRPv, for March in the Arctic (a) and for September in the Antarctic (b). Large dots, empty circles and small dots indicate areas where the BRP applies to 100%, more than 50% and less than 50% of the salt rejected by sea ice, respectively. The BRP is not applied in areas without symbols.

Although this simple refinement of the BRP improves the simulated MLDs, it also brings new significant sources of uncertainty. In particular, a proper behavior of the parameterization relies on a correct representation of both the sea ice circulation and the ocean surface currents. Furthermore, the choice of the velocity thresholds used to separate the different mixing regimes is rather arbitrary. They could be considered as ad hoc model tuning parameters.

5. Conclusions

In this study, a brine rejection parameterization has been introduced in the global ocean–sea ice model NEMO-LIM3. The aim of this parameterization is to mimic the effects of small-scale convection associated with intense brine rejections in leads in winter, and to avoid excessive grid-scale mixing. The basic principle is to distribute the salt rejected by sea ice according to a power-law profile within the mixed layer, a greater fraction being deposited at its base than at the surface. Model results were validated against two recently published products, namely a mixed layer depth climatology and a hydrographic dataset derived from seal-borne CTD sensors.

The main effect of the parameterization is to reduce significantly the mixed layer depth in ice-covered areas. Salinity decreases at the surface and marginally increases in the subsurface. Less heat is lost to the atmosphere in autumn and winter, due to the reduced vertical mixing, inducing an increase in upper-ocean temperature. In the Antarctic, the oceanic changes are large enough as to impact the sea ice thickness, although the atmospheric forcing is prescribed.

While mixed layer depths are locally in the Northern Hemisphere in better agreement with observational estimates, the reduction in surface mixing is in general too strong, hence degrading model results in most regions. Uncertainties in the comparison to observations and inaccuracies in the representation of other mixing processes prevent a definitive attribution of these biases to the brine rejection parameterization itself. However, in the way it is first applied here, all brine rejections from sea ice are unrealistically turned into a process which restratifies the mixed layer, without any deepening effect left.

In reality, salt plumes are likely to occur only for low ice–ocean relative velocities, otherwise shear-driven mixing is dominant over convective mixing, and for the salt rejected in a localized manner, which is not easy to identify in a model. Including a dependency on the relative velocities has been tested and shown to yield clear improvements in the simulated mixed layer depths. Yet, this comes at the price of introducing new poorly constrained parameters in the design of the parameterization. A more explicit approach is possible and promising. Following Holland (2003), the ice–ocean fluxes can be differentiated at the subgrid-scale across sea ice categories and open water, and the oceanic conditions and mixing regimes below each category can be represented. This is the subject of ongoing work.

Acknowledgments

We thank two anonymous reviewers for their valuable comments on the original manuscript. A. Barthélemy and H. Goosse are Research Assistant and Senior Research Associate with the Fonds National de la Recherche Scientifique (F.R.S.-FNRS/Belgium), respectively. We are grateful to F. Roquet and S. Schmidtko for making the MEOP-CTD database and the MIMOC climatology readily available. Computational resources have been provided by the supercomputing facilities of the Université catholique de Louvain (CISM/UCL) and the Consortium des Equipements de Calcul Intensif en Fédération Wallonie Bruxelles (CECI) funded by the F.R.S.-FNRS/Belgium under convention 2.5020.11.

References

Adcroft, A., Hill, C., Marshall, J., 1997. Representation of topography by shaved cells in a height coordinate ocean model. Mon. Weather Rev. 125, 2293–2315. http://dx.doi.org/10.1175/1520-0493(1997)125<2293:ROTBSC>2.0.CO;2.

Blanke, B., Delecluse, P., 1993. Variability of the tropical Atlantic Ocean simulated by a general circulation model with two different mixed-layer physics. J. Phys. Oceanogr. 23, 1363–1388. http://dx.doi.org/10.1175/1520-0485(1993)023<1363:VOTTAO>2.0.CO;2.

Bouttes, N., Paillard, D., Roche, D.M., 2010. Impact of brine-induced stratification on the glacial carbon cycle. Clim. Past 6, 575–589. http://dx.doi.org/10.5194/cp-6-575-2010.

Calvert, D., Siddorn, J., 2013. Revised vertical mixing parameters for the UK community standard configuration of the global NEMO ocean model. Technical Note 95. Met Office Hadley Centre. United Kingdom.

Comiso, J.C., 2000. Bootstrap Sea Ice Concentrations from Nimbus-7 SMMR and DMSP SSM/I-SSMIS. Version 2. [1983–2012]. NASA DAAC at the National Snow and Ice Data Center. Boulder, Colorado, USA.

Conkright, M.E., Locarnini, R.A., Garcia, H.E., O'Brien, T.D., Boyer, T.P., Stephens, C., Antonov, J.I., 2002. World Ocean Atlas 2001 Digital Media. National Oceanographic Data Center, Silver Spring, Maryland, USA.

de Boyer Montégut, C., Madec, G., Fischer, A.S., Lazar, A., Iudicone, D., 2004. Mixed layer depth over the global ocean: an examination of profile data and a profile-based climatology. J. Geophys. Res. 109, C12003. http://dx.doi.org/10.1029/2004JC002378.

Duffy, P.B., Caldeira, K., 1997. Sensitivity of simulated salinity in a three-dimensional ocean model to upper ocean transport of salt from sea–ice formation. Geophys. Res. Lett. 24, 1323–1326. http://dx.doi.org/10.1029/97GL01294.

Duffy, P.B., Eby, M., Weaver, A.J., 1999. Effects of sinking of salt rejected during formation of sea ice on results of an ocean–atmosphere–sea ice climate model. Geophys. Res. Lett. 26, 1739–1742. http://dx.doi.org/10.1029/1999GL900286.

Fox-Kemper, B., Danabasoglu, G., Ferrari, R., Griffies, S., Hallberg, R., Holland, M., Maltrud, M., Peacock, S., Samuels, B., 2011. Parameterization of mixed layer eddies. III: implementation and impact in global ocean climate simulations. Ocean Modell. 39, 61–78. http://dx.doi.org/10.1016/j.ocemod.2010.09.002.

Gent, P.R., Mcwilliams, J.C., 1990. Isopycnal mixing in ocean circulation models. J. Phys. Oceanogr. 20, 150–155. http://dx.doi.org/10.1175/1520-0485(1990)020<0150:IMIOCM>2.0.CO;2.

Goosse, H., 1997. Modelling the Large-Scale Behaviour of the Coupled Ocean–Sea–Ice System (Ph.D. thesis). Université catholique de Louvain.

Goosse, H., Fichefet, T., 1999. Importance of ice–ocean interactions for the global ocean circulation: a model study. J. Geophys. Res. 104, 23337–23355. http://dx.doi.org/10.1029/1999JC900215.

Holland, M.M., 2003. An improved single-column model representation of ocean mixing associated with summertime leads: results from a SHEBA case study. J. Geophys. Res. 108, 3107. http://dx.doi.org/10.1029/2002JC001557.

Holland, P.R., Bruneau, N., Enright, C., Losch, M., Kurtz, N.T., Kwok, R., 2014. Modeled trends in Antarctic sea ice thickness. J. Clim. 27, 3784–3801. http://dx.doi.org/10.1175/JCLI-D-13-00301.1.

Holte, J., Talley, L., 2009. A new algorithm for finding mixed layer depths with applications to argo data and subantarctic mode water formation. J. Atmos. Oceanic Technol. 26, 1920–1939. http://dx.doi.org/10.1175/2009JTECHO543.1.

Huang, C.J., Qiao, F., Dai, D., 2014. Evaluating CMIP5 simulations of mixed layer depth during summer. J. Geophys. Res. Oceans 119, 2568–2582. http://dx.doi.org/10.1002/2013JC009535.

Jackson, J.M., Williams, W.J., Carmack, E.C., 2012. Winter sea–ice melt in the Canada Basin, Arctic Ocean. Geophys. Res. Lett. 39, L03603. http://dx.doi.org/10.1029/2011GL050219.

Jin, M., Hutchings, J., Kawaguchi, Y., Kikuchi, T., 2012. Ocean mixing with lead-dependent subgrid scale brine rejection parameterization in a climate model. J. Ocean Univ. China 11, 473–480. http://dx.doi.org/10.1007/s11802-012-2094-4.

Kalnay, E., Kanamitsu, M., Kistler, R., Collins, W., Deaven, D., Gandin, L., Iredell, M., Saha, S., White, G., Woollen, J., Zhu, Y., Leetmaa, A., Reynolds, R., Chelliah, M., Ebisuzaki, W., Higgins, W., Janowiak, J., Mo, K.C., Ropelewski, C., Wang, J., Jenne, R., Joseph, D., 1996. The NCEP/NCAR 40-year reanalysis project. Bull. Am. Meteor. Soc. 77, 437–471. http://dx.doi.org/10.1175/1520-0477(1996)077<0437:TNYRP>2.0.CO;2.

Kantha, L.H., 1995. A numerical model of Arctic leads. J. Geophys. Res. 100, 4653–4672. http://dx.doi.org/10.1029/94JC02348.

Kim, S.J., Stössel, A., 2001. Impact of subgrid-scale convection on global thermohaline properties and circulation. J. Phys. Oceanogr. 31, 656–674. http://dx.doi.org/10.1175/1520-0485(2001)031<0656:IOSSCO>2.0.CO;2.

Komuro, Y., 2014. The impact of surface mixing on the Arctic river water distribution and stratification in a global ice–ocean model. J. Clim. 27, 4359–4370. http://dx.doi.org/10.1175/JCLI-D-13-00090.1.

Krishfield, R., Toole, J., Proshutinsky, A., Timmermans, M.L., 2008. Automated ice-tethered profilers for seawater observations under pack ice in all seasons. J. Atmos. Oceanic Technol. 25, 2091–2105. http://dx.doi.org/10.1175/2008JTECHO587.1.

Madec, G., 2008. NEMO ocean engine. Note du Pôle de modélisation 27. Institut Pierre-Simon Laplace. France. ISSN No 1288–1619.

Madec, G., Imbard, M., 1996. A global ocean mesh to overcome the North Pole singularity. Clim. Dyn. 12, 381–388. http://dx.doi.org/10.1007/BF00211684.

Massonnet, F., Fichefet, T., Goosse, H., Vancoppenolle, M., Mathiot, P., König Beatty, C., 2011. On the influence of model physics on simulations of Arctic and Antarctic sea ice. The Cryosphere 5, 687–699. http://dx.doi.org/10.5194/tc-5-687-2011.

Massonnet, F., Mathiot, P., Fichefet, T., Goosse, H., König Beatty, C., Vancoppenolle, M., Lavergne, T., 2013. A model reconstruction of the Antarctic sea ice thickness and volume changes over 1980–2008 using data assimilation. Ocean Modell. 64, 67–75. http://dx.doi.org/10.1016/j.ocemod.2013.01.003.

Matsumura, Y., Hasumi, H., 2008. Brine-driven eddies under sea ice leads and their impact on the Arctic Ocean mixed layer. J. Phys. Oceanogr. 38, 146–163. http://dx.doi.org/10.1175/2007JPO3620.1.

Maykut, G.A., 1978. Energy exchange over young sea ice in the central Arctic. J. Geophys. Res. 83, 3646–3658. http://dx.doi.org/10.1029/JC083iC07p03646.

Morison, J.H., McPhee, M.G., 1998. Lead convection measured with an autonomous underwater vehicle. J. Geophys. Res. 103, 3257–3281. http://dx.doi.org/10.1029/97JC02264.

Morison, J.H., McPhee, M.G., Curtin, T.B., Paulson, C.A., 1992. The oceanography of winter leads. J. Geophys. Res. 97, 11199–11218. http://dx.doi.org/10.1029/92JC00684.

Muench, R.D., Smith, D.C., Paulson, C.A., 1995. Convection beneath freezing leads: new observations compared with numerical model results. J. Geophys. Res. 100, 4681–4692. http://dx.doi.org/10.1029/94JC02503.

Nguyen, A.T., Menemenlis, D., Kwok, R., 2009. Improved modeling of the Arctic halocline with a subgrid-scale brine rejection parameterization. J. Geophys. Res. 114, C11014. http://dx.doi.org/10.1029/2008JC005121.

Petty, A.A., Holland, P.R., Feltham, D.L., 2014. Sea ice and the ocean mixed layer over the Antarctic shelf seas. The Cryosphere 8, 761–783. http://dx.doi.org/10.5194/tc-8-761-2014.

Rodgers, K.B., Aumont, O., Mikaloff Fletcher, S.E., Plancherel, Y., Bopp, L., de Boyer Montégut, C., Iudicone, D., Keeling, R.F., Madec, G., Wanninkhof, R., 2014. Strong sensitivity of Southern Ocean carbon uptake and nutrient cycling to wind stirring. Biogeosciences 11, 4077–4098. http://dx.doi.org/10.5194/bg-11-4077-2014.

Roquet, F., Charrassin, J.B., Marchand, S., Boehme, L., Fedak, M., Reverdin, G., Guinet, C., 2011. Delayed-mode calibration of hydrographic data obtained from animal-borne satellite relay data loggers. J. Atmos. Oceanic Technol. 28, 787–801. http://dx.doi.org/10.1175/2010JTECHO801.1.

Roquet, F., Wunsch, C., Forget, G., Heimbach, P., Guinet, C., Reverdin, G., Charrassin, J.B., Bailleul, F., Costa, D.P., Huckstadt, L.A., Goetz, K.T., Kovacs, K.M., Lydersen, C., Biuw, M., Nøst, O.A., Bornemann, H., Ploetz, J., Bester, M.N., McIntyre, T., Muelbert, M.C., Hindell, M.A., McMahon, C.R., Williams, G., Harcourt, R., Field, I.C., Chafik, L., Nicholls, K.W., Boehme, L., Fedak, M.A., 2013. Estimates of the Southern Ocean general circulation improved by animal-borne instruments. Geophys. Res. Lett. 40. http://dx.doi.org/10.1002/2013GL058304 (2013GL058304).

Schmidtko, S., Johnson, G.C., Lyman, J.M., 2013. MIMOC: a global monthly isopycnal upper-ocean climatology with mixed layers. J. Geophys. Res. Oceans 118, 1658–1672. http://dx.doi.org/10.1002/jgrc.20122.

Schweiger, A., Lindsay, R., Zhang, J., Steele, M., Stern, H., Kwok, R., 2011. Uncertainty in modeled Arctic sea ice volume. J. Geophys. Res. 116, C00D06. http://dx.doi.org/10.1029/2011JC007084.

Skyllingstad, E.D., Denbo, D.W., 2001. Turbulence beneath sea ice and leads: a coupled sea ice/large-eddy simulation study. J. Geophys. Res. 106, 2477–2497. http://dx.doi.org/10.1029/1999JC000091.

Smith, D.C., Morison, J.H., 1993. A numerical study of haline convection beneath leads in sea ice. J. Geophys. Res. 98, 10069–10083. http://dx.doi.org/10.1029/93JC00137.

Smith, D.C., Morison, J.H., 1998. Nonhydrostatic haline convection under leads in sea ice. J. Geophys. Res. 103, 3233–3247. http://dx.doi.org/10.1029/97JC02262.

Smith, W.O., Dinniman, M.S., Hofmann, E.E., Klinck, J.M., 2014. The effects of changing winds and temperatures on the oceanography of the Ross Sea in the 21st century. Geophys. Res. Lett. 41, 1624–1631. http://dx.doi.org/10.1002/2014GL059311.

Steele, M., Morley, R., Ermold, W., 2001. PHC: a global ocean hydrography with a high-quality Arctic Ocean. J. Clim. 14, 2079–2087. http://dx.doi.org/10.1175/1520-0442(2001)014<2079:PAGOHW>2.0.CO;2.

Vancoppenolle, M., Fichefet, T., Goosse, H., 2009. Simulating the mass balance and salinity of Arctic and Antarctic sea ice. 2. Importance of sea ice salinity variations. Ocean Modell. 27, 54–69. http://dx.doi.org/10.1016/j.ocemod.2008.11.003.

Vancoppenolle, M., Meiners, K.M., Michel, C., Bopp, L., Brabant, F., Carnat, G., Delille, B., Lannuzel, D., Madec, G., Moreau, S., Tison, J.L., van der Merwe, P., 2013. Role of sea ice in global biogeochemical cycles: emerging views and challenges. Quaternary Sci. Rev. 79, 207–230. http://dx.doi.org/10.1016/j.quascirev.2013.04.011.

Worby, A.P., Geiger, C.A., Paget, M.J., Van Woert, M.L., Ackley, S.F., DeLiberty, T.L., 2008. Thickness distribution of Antarctic sea ice. J. Geophys. Res. 113, C05S92. http://dx.doi.org/10.1029/2007JC004254.

Zhang, J., Steele, M., 2007. Effect of vertical mixing on the Atlantic water layer circulation in the Arctic Ocean. J. Geophys. Res. 112, C04S04. http://dx.doi.org/10.1029/2006JC003732.

Zhang, J., Lindsay, R., Schweiger, A., Steele, M., 2013. The impact of an intense summer cyclone on 2012 Arctic sea ice retreat. Geophys. Res. Lett. 40, 720–726. http://dx.doi.org/10.1002/grl.50190.